Journal of Solid State Chemistry **157,** 324–338 (2001)
doi:10.1006/jssc.2000.9073, available online at http://www.idealibrary.com on IDEAL®

Metathesis Reactions of the *super*-Prussian Blue Systems $[(Me_3Sn)_3M(CN)_6]$ (M = Co, Ir) with, *inter alia*, Tetrapropylammonium (and -phosphonium) Ions: Crystal Structures of $[(nPr_4P)(Me_3Sn)_2Co(CN)_6 \cdot 2H_2O]$ and $[(nPr_4N)(Me_3Sn)_2Ir(CN)_6 \cdot 2H_2O]$

Eyck-Michael Poll,* Falk Olbrich,† Sabine Samba,* R. Dieter Fischer,*,[1] Paolo Avalle,‡ David C. Apperley,‡ and Robin K. Harris‡,[2]

*Institut für Anorganische und Angewandte Chemie der Universität Hamburg, Martin-Luther-King-Platz 6, 20146 Hamburg, Germany; †Chemisches Institut, Otto-von-Guericke-Universität Magdeburg, Universitätsplatz 2, 39106 Magdeburg, Germany; and ‡Department of Chemistry, University of Durham, South Road, Durham DH1 3LE, England

Received August 29, 2000; in revised form December 4, 2000; accepted December 8, 2000; published online February 19, 2001

Tetrapropylammonium and -phosphonium ions, nPr_4E^+, react readily with the polymeric *super*-Prussian blue derivatives $[(Me_3Sn)_3M(CN)_6]$ (M = Co, Ir), which are built up of infinite $\dashv M{-}CN{-}Sn{-}NC\vdash$ chains, affording the *dimorphic* supramolecular assembly $[(nPr_4E)(Me_3Sn)_2M(CN)_6 \cdot 2H_2O]$. All representatives of the latter type are devoid of any extended $\dashv M{-}CN{-}Sn{-}NC\vdash$ backbones. The single-crystal X-ray structures of 1a-P (E = P; M = Co) and 3a (E = *N*; M = Ir) document new examples of either modification. While Me_4N^+ and Et_4N^+ ions do not form sufficiently insoluble, R_4N^+-containing assemblies, nBu_4N^+ and $nPen_4N^+$ give rise to similar (i.e., $R_4N : Me_3Sn = 1 : 2$) products as nPr_4N^+. The slightly modified *super*-Prussian blue system $[\{Me_2Sn(CH_2)_3SnMe_2\}_{1.5}Co(CN)_6]$, 4, reacts with nPr_4NBr to yield the assembly $[(nPr_4N)\{Me_2Sn(CH_2)_3SnMe_2\}Co(CN)_6 \cdot 2H_2O]$, 4a, the powder XRD and solid-state NMR spectra of which strongly resemble those of 3a (with two *cis*-oriented $CNSn(Me_3)OH_2$ ligands). In the absence of suitable single crystals, in particular in the case M = Ir, powder XRD- and multinuclear solid-state NMR results have been carefully examined in view of specific similarities with already established structural patterns. The unexpected dimorphism of 1a, which has been described most recently for M = Co, could now also be confirmed for M = Ir. The experimental results of the present study in total indicate that the superiority of coordinative $N \rightarrow Sn$ bonds over $O \rightarrow Sn$ bonds, in combination with $O{-}H \cdots N \equiv C$ hydrogen bridges, decreases, in the presence of R_4E^+ ions, stepwise with the size of R (i.e., from methyl to *n*-propyl) and of M (i.e., Co vs Ir).

© 2001 Academic Press

[1]E-mail: fischer@chemie.uni-hamburg.de. Fax: (+49) 40-42838-2882.
[2]E-mail: R.K.Harris@durham.ac.uk. Fax: (+44) 191-386-1127.

INTRODUCTION

While alkaline and alkaline earth metal ions may readily be *recognized* by tailor-made acceptors such as *coronands* and *cryptands* (1), possibilities of selectively recognizing tetraalkylammonium ions, R_4N^+, have remained more limited. Apart from several molecular receptors (2), polymeric frameworks such as zeolites are likely to function as specific hosts of distinct R_4N^+ (and R_4P^+) ions, too, particularly when these cations are adopted as *templates* during the synthesis of zeolites (3). While, however, structural details about *as-prepared* (i.e., noncalcined) zeolites are still scarce (4), there is increasing evidence that polymeric metal cyanides may serve as suitable R_4E^+ acceptors. For instance, the reaction of $Hg(CN)_2$ with MCN (M = Li, Na, K) and R_4NCN in H_2O affords precipitates of different $Hg/M/R_4N$ ratios, depending essentially on the size of the alkyl group R (5). We have shown recently that coordination polymers of the *super*-Prussian blue type $[(Me_3Sn)_3M(CN)_6] \equiv {}^3_\infty[M\{\mu\text{-}CNSn(Me_3)NC\}_3]$ with M = Fe and Co (6) may undergo facile cation exchange according to

$$[(Me_3Sn)_3M(CN)_6] + R_4N^+ \xrightarrow{(H_2O)} [(R_4N)(Me_3Sn)_2M(CN)_6 \cdot xH_2O] + Me_3Sn \cdot aq^+, \quad [1]$$

affording with R = *n*-propyl (*n*Pr), *n*-butyl (*n*Bu), and *n*-pentyl (*n*Pen), respectively, again sparingly water-soluble, although water-containing products of surprisingly versatile structures (7,8). Coordinative $H_2O \rightarrow Sn$ and $CN \rightarrow Sn$ interactions as well as $OH_2 \cdots NC$ and eventually even weak $CH_2 \cdots NC$ hydrogen bonds appear to be responsible for

0022-4596/01 $35.00
Copyright © 2001 by Academic Press
All rights of reproduction in any form reserved.

the generation of the various structural designs. Most interestingly, only the $n\mathrm{Pr}_4\mathrm{N}^+$ ion was found to completely abandon the otherwise preferred motif of infinite or finite $[M\text{–CN–Sn–NC}]_n$ chains (8). To examine how significantly a subtle tuning of the basic building blocks R_4E^+, $[M(\mathrm{CN})_6]^{3-}$, and $\mathrm{Me}_3\mathrm{Sn}^+$, respectively, may affect the concerted structure-directing influence of the various comparatively weak modes of interaction, the present study is extended particularly toward the related building blocks $n\mathrm{Pr}_4P^+$ and $[Ir(\mathrm{CN})_6]^{3-}$, respectively. Moreover, the starting polymer $[(\mathrm{Me}_3\mathrm{Sn})_3\mathrm{Co}(\mathrm{CN})_6]$ (**1**) was complemented by its slightly modified derivative $[\{\mathrm{Me}_2\mathrm{Sn}(\mathrm{CH}_2)_3\mathrm{SnMe}_2\}_{1.5}\mathrm{Co}(\mathrm{CN})_6]$ (**4**), wherein the tin atoms are tied pairwise together by a trimethylene bridge (9).

Instead of using throughout the lengthy formulae of the various products expected according to Eq. [1], the following shorthand notation will be used: The basic *super*-Prussian blue homologues $[(\mathrm{Me}_3\mathrm{Sn})_3M(\mathrm{CN})_6]$ with $M = \mathrm{Co}$, Fe, and Ir, as well as the derivative $[\{\mathrm{Me}_2\mathrm{Sn}(\mathrm{CH}_2)_3\mathrm{SnMe}_2\}_{1.5}\mathrm{Co}(\mathrm{CN})_6]$, are designated simply by **1**, **2**, **3**, and **4**, respectively. Metathesis (or co-precipitation, see Eq. [2]) products of **1**–**3** of the general type: $[(R_4\mathrm{N})(\mathrm{Me}_3\mathrm{Sn})_2M(\mathrm{CN})_6\cdot x\mathrm{H}_2\mathrm{O}]$ and of **4**, respectively, of the type $[(R_4E)\{\mathrm{Me}_2\mathrm{Sn}(\mathrm{CH}_2)_3\mathrm{SnMe}_2\}\mathrm{Co}(\mathrm{CN})_6\cdot x\mathrm{H}_2\mathrm{O}]$ are specified by an additional letter, e.g., by **a** for $R = n\mathrm{Pr}$, **b** for $R = n\mathrm{Bu}$, and **c** for $R = n\mathrm{Pen}$. In cases where $E = \mathrm{P}$ (but not N), the symbol will also include a **P**. For instance, **3a-P** stands for $[(n\mathrm{Pr}_4\mathbf{P})(\mathrm{Me}_3\mathrm{Sn})_2\mathbf{Ir}(\mathrm{CN})_6\cdot x\mathrm{H}_2\mathrm{O}]$. Although most of the products could, in principle, be prepared both according to Eq. [1] and by co-precipitation,

$$R_4\mathrm{N}^+ + 2\mathrm{Me}_3\mathrm{Sn}\cdot\mathrm{aq}^+ + [M(\mathrm{CN})_6]^{3-} + x\mathrm{H}_2\mathrm{O} \rightarrow [(R_4\mathrm{N})(\mathrm{Me}_3\mathrm{Sn})_2M(\mathrm{CN})_6\cdot x\mathrm{H}_2\mathrm{O}]\downarrow, \quad [2]$$

the two routes lead in few cases to nonequivalent products, which will be specified more clearly in the following. It is important to point out that the notation adopted here is not identical to that used in our previous contributions (7, 8).

EXPERIMENTAL

Materials

$\mathrm{K}_3[\mathrm{Ir}(\mathrm{CN})_6]$ (IR, ν(CN): 2134 cm^{-1}), $n\mathrm{Pr}_4\mathrm{PBr}$, and $[\{\mathrm{Me}_2\mathrm{Sn}(\mathrm{CH}_2)_3\mathrm{SnMe}\}_{1.5}\mathrm{Co}(\mathrm{CN})_6]$ (**4**) were prepared according to Refs. (10, 11, 9), respectively.

$[(\mathrm{Me}_3\mathrm{Sn})_3\mathrm{Ir}(\mathrm{CN})_6]$, **3** (12): A solution of 0.70 g (3.5 mmol) of $\mathrm{Me}_3\mathrm{SnCl}$ in 10 mL of $\mathrm{H}_2\mathrm{O}$ was added under stirring to a solution of 0.47 g (1.0 mmol) of $\mathrm{K}_3[\mathrm{Ir}(\mathrm{CN})_6]$ in 10 mL of $\mathrm{H}_2\mathrm{O}$. After filtration, washing of the white residue with a small portion of cold $\mathrm{H}_2\mathrm{O}$ and drying (oil pump), 0.7 g (yield: 90%) of analytically pure **3** was obtained. ν(CN) bands (cm^{-1}, IR/Raman): 2156 vs/2208 w, 2179 w. Decomposition temperature ≥ 330°C.

Anal. Calcd for $\mathrm{C}_{15}\mathrm{H}_{27}\mathrm{N}_6\mathrm{IrSn}_3$ (839.69): C 21.45, H 3.24, N 10.70, Sn 42.41; found C 21.91, H 3.77, N 10.04, Sn 38.22%.

As in the presence of Ir, the special disintegration procedure developed in our laboratory for the analysis of Sn did not afford strictly clear solutions; the experimental Sn values of **3** and its derivatives generally turned out to be too low. Unit cell parameters of **1** and **3** for space group $C2/c$ from powder X-ray diffractograms (12b): *a*, 16.825(5)/17.155(3) Å; *b*, 12.892(4)/13.210(3) Å; *c*, 14.686(4)/14.858(3) Å; β, 106.86(3)/107.64(2)°.

$[(R_4\mathrm{N})(\mathrm{Me}_3\mathrm{Sn})_2\mathrm{M}(\mathrm{CN})_6\cdot m\mathrm{H}_2\mathrm{O}]$ systems (see Scheme 1); (**3a**) 97 mg (0.1 mmol) of **3** was suspended in a solution of 26 mg (0.1 mmol) of $n\mathrm{Pr}_4\mathrm{NCl}$ in 20 mL of $\mathrm{H}_2\mathrm{O}$. After stirring, filtration, washing (by small portions of cold $\mathrm{H}_2\mathrm{O}$), and drying, 50 mg (yield: 50%) of a white, polycrystalline material was obtained. ν(CN) bands (IR, cm^{-1}): 2147 vs, 2138 vs. Decomposition temperature ≥ 305°C (generation of a yellow, solid foam).

Anal. Calcd for $\mathrm{C}_{24}\mathrm{H}_{50}\mathrm{N}_7\mathrm{O}_2\mathrm{IrSn}_2$ (898.26): C 32.09, H 5.61, N 10.91; found C 31.77, H 5.56, N 10.66%.

(**3b**) Procedure analogous to that employed for **3a**; **3**, 91 mg (0.1 mmol); $n\mathrm{Bu}_4\mathrm{NBr}$, 35 mg (0.1 mmol); yield: 57 mg (57%). ν(CN) band (IR, cm^{-1}): 2142 vs.

Anal. Calcd for $\mathrm{C}_{28}\mathrm{H}_{56}\mathrm{N}_7\mathrm{OIrSn}_2$ (936.38): C 35.92, H 6.03, N 10.47; found C 35.14, H 6.21, N 10.18%.

(**1a-P**) Procedure analogous to that described for **3a**; **1**, 300 mg (0.4 mmol), $n\mathrm{Pr}_4\mathrm{PBr}$, 120 mg (0.4 mmol) in ca. 30 mL of $\mathrm{H}_2\mathrm{O}$. Yield: 150 mg (ca. 50%); ν(CN) bands (IR/Raman, cm^{-1}): 2152 vs, 2139 vs/2172 vs, 2153 s, 2140 m-w; decomposition temperature 295°C (blue), 330°C (black).

Anal. Calcd for $\mathrm{C}_{24}\mathrm{H}_{50}\mathrm{N}_6\mathrm{O}_2\mathrm{CoPSn}_2$ (781.99): C 36.86, H 6.44, N 10.74, O 4.09, P 3.96, Co 7.54, Sn 30.35; found C 36.62, H 6.22, N 10.62, O 3.60, P 3.68, Co 7.43, Sn 30.42%.

(**3a-P**) **3**, 300 mg (0.35 mmol), $n\mathrm{Pr}_4\mathrm{PBr}$, 101 mg (0.35 mmol) in ca. 30 mL of $\mathrm{H}_2\mathrm{O}$; yield: 150 mg (ca. 50%). ν(CN) band (IR, cm^{-1}): 2146 vs; decomposition temperature 340°C (gray).

Anal. Calcd for $\mathrm{C}_{24}\mathrm{H}_{50}\mathrm{N}_6\mathrm{O}_2\mathrm{PIrSn}_2$ (915.25): C 31.49, H 5.51, N 9.18; found C 31.06, H 5.01, N 8.89%.

(**3c** ($x = 2$)) **3**, 100 mg (0.1 mmol); $n\mathrm{Pen}_4\mathrm{NBr}$, 45 mg (0.1 mmol); 20 mL of $\mathrm{H}_2\mathrm{O}$; yield: 50 mg (ca. 50%); decomposition temperature 290°C (faintly yellow), 340°C (deep yellow).

Anal. Calcd for $\mathrm{C}_{32}\mathrm{H}_{66}\mathrm{N}_7\mathrm{O}_2\mathrm{IrSn}_2$ (1010.51): C 38.03, H 6.58, N 9.70; found C 37.68, H 6.25, N 9.47%.

(**4a**) **4** (9), 100 mg (0.138 mmol); $n\mathrm{Pr}_4\mathrm{NCl}$, 30.61 mg (0.138 mmol) in 100 mL of $\mathrm{H}_2\mathrm{O}$ (plus a few drops of MeCN), reaction time: 24 h. Yield: 80 mg (75%); ν(CN) bands (IR, cm^{-1}): 2139 vs, 2145 vs; decomposition temperature ca. 280°C (blue).

Anal. Calcd for $\mathrm{C}_{25}\mathrm{H}_{50}\mathrm{N}_7\mathrm{O}_2\mathrm{CoSn}_2$ (777.03): C 38.64, H 6.486, N 12.61; found C 37.78, H 6.28, N 12.34% (corre-

sponding values were found for **4a** obtained by co-precipitation). ^{1}H NMR (200 MHz, D_2O/NaOD, pH ca. 9): $\delta = 0.36$ (s, 12 H, CH_3Sn), 1.19 (t, 4 H CH_2Sn), 1.97 (pentet, 2 H, $-CH_2-$), 3.16 (pentet, 8 H, α-CH_2N), 1.70 (septet, 8 H, β-CH_2), 0.94 (t, 12 H, γ-CH_3); $J(^{119}Sn, ^{13}C)$: 60 ± 1 Hz.

(**4b**) Synthesis according to that of **1a** (by co-precipitation) (8) from aqueous solutions of $K_3[Co(CN)_6]$ (73.1 mg, 0.22 mmol) in H_2O (ca. 10 mL), and nBu$_4$NCl (61.1 mg, 0.22 mmol) and $(Me_2SnBr)_2(CH_2)_3$ (117.2 mg, 0.234 mmol) in H_2O (ca. 20 mL). Yield: 170 mg (ca. 93%). ν(CN) band (IR, cm^{-1}): 2136; decomposition temperature 300°C (light blue), 340°C (dark blue). ^{1}H NMR (200 MHz, D_2O/NaOD, pH ca. 9): δ (ppm) 0.37 (s, 12H, CH_3Sn), 1.20 (t, 4H, CH_2Sn), 1.99 (pentet, 2H, $-CH_2-$), 3.20 (m, 8H, α-CH_2N), 1.65 (m, 8H, β-CH_2), 1.35 (m, 8H, γ-CH_2), 0.94 (t, 12H, δ-CH_3); $J(^{119}Sn, ^{13}C)$ of CH_3Sn: 52 Hz.

Methods

Correct R_4E/Me_3Sn ratios of all R_4E-containing samples were deduced independently by inspection of the ^{1}H NMR spectra of solutions in D_2O/NaOD (pH of $\approx$9–12, see the exemplaric data for **4a** and **4b** listed above). NMR spectrometers used for liquid samples were either Varian Gemini 200 BB or Bruker AM 360. Infrared spectra were obtained on a Perkin–Elmer IR-1720 spectrometer and Raman spectra on a Jobin Yvon U-1000 instrument.

Single crystals suitable for X-ray crystallography were recovered from the filtrates obtained during the syntheses of **3a** and **1a-P** (*vide supra*). Crystal structure determinations were performed on a Siemens axs Smart-CCD diffractometer (see also Table 2). Absorption corrections based on symmetry equivalent reflections using the SADABS program were solved by direct methods and refined by a full-matrix least-squares procedure against F^2 with SHELXS-97 and SHELXL-97. Crystallographic data for **1a-P** and **3a** have been deposited with the Cambridge Crystallographic Data Centre.[3]

X-ray powder diffractograms (XRDs) were obtained either on a Philips PW 1050 or a Bruker D8 Advance instrument (with Cu$K\alpha$ source and Ni filter). Powder diagrams were simulated with CERIUS^2 4.0 (of MSI Inc.), for the 2θ range 5°–70°.

Solid-state NMR: Most of the solid-state NMR spectra were recorded on a Varian Unity Plus 300 spectrometer operating at frequencies of 75.4, 121.4, and 111.9 MHz for ^{13}C, ^{31}P, and ^{119}Sn, respectively. Cross-polarization with high-power proton decoupling was used for all spectra. The ^{13}C and ^{31}P spectra were recorded employing a Doty Scientific probe with 7-mm o.d. rotors, but for the ^{119}Sn spectra a Doty Scientific probe with 5-mm o.d. rotors was used. Typical spectrometer operating conditions were as follows.

For ^{13}C: Contact time, 1.0–8.0 ms; recycle delays, 1.5–3.0 s; number of transients, 2400–26,300 (the higher values being necessary to obtain excellent S/N for the cyanide resonances); spin rates, 4.0–9.0 kHz.

For ^{119}Sn: Contact times, 1.0–5.0 ms; recycle delays, 2.0–5.0 s; number of transients, 2000–31,800; spin rates, 4.0–8.2 kHz.

For ^{31}P: Contact times, 1.0 ms; recycle delays, 1.0 s; number of transients, 4–120; spin rates, 5.9–7.2 kHz.

All spectra were obtained at ambient probe temperature (uncalibrated). Chemical shifts are reported, with the high-frequency-positive convention, in ppm relative to the signals for $SiMe_4$, $SnMe_4$, and 85% aq. H_3PO_4 for ^{13}C, ^{119}Sn, and ^{31}P, respectively. Shielding tensor components are defined by $|\sigma_{ZZ} - \sigma_{iso}| \geq |\sigma_{XX} - \sigma_{iso}| \geq |\sigma_{YY} - \sigma_{iso}|$, with anisotropy $\xi = \sigma_{ZZ} - \sigma_{iso}$ and asymmetry $\eta = (\sigma_{YY} - \sigma_{XX})/\xi$. Analysis of spinning sideband manifolds was carried out using either an in-house computer program (13) or the STARS Varian software.

RESULTS

*Preparation and General Properties of **3**, **3a**, **3b**, **3c**, **1a-P**, **3a-P**, **4a**, and **4b***

Although the anhydrous *super*-Prussian blue derivative **3** (M = Ir) was obtained in reasonable yields in the same way as its longer known homologues **1** and **2** (i.e., from concentrated aqueous solutions; see Experimental Section), its solubility in water turned out to be significantly higher than that of **1**. Thus, a few milligrams of **3** could be redissolved in at most 50 mL of pure water after violent stirring for about 30 min, while more than 100 mL were necessary to dissolve the corresponding equivalent of **1**. The notably better solubility of **3** is even exceeded by that of its hypothetic lead-containing homologue, $[(Me_3Pb)_3Ir(CN)_6]$, which does not precipitate from a weakly acidic aqueous solution of Me_3PbCl after addition of a concentrated solution of $K_3[Ir(CN)_6]$ (12a). The X-ray powder diffractogram (XRD) of **3** resembles strongly the XRDs of **1** and **2**, manifesting that again infinite $\{Ir–CN–Sn–NC\}$ chains constitute a corresponding 3-D framework for **3** as known for **1** (6, 11). However, in surprising contrast to our earlier findings (7, 8), according to which suspensions of **1** and **2** in solutions containing the ion Me_4N^+ or Et_4N^+ remain completely unchanged, **3** is found to redissolve completely in solutions of the salts Me_4NI or Et_4NCl.

On the other hand, a suspension of **3** in aqueous solutions of nPr$_4$NCl and nPr$_4$PBr, respectively, affords in acceptable yields (i.e., of ca. 50%) the new, sparingly water-soluble products **3a** and **3a-P**. Correspondingly, **3b** could also be obtained from **3** and nBu$_4$NBr. Somewhat more surprisingly,

[3]Copies may be obtained free of charge on application to the Director, CCDC, 12 Union Road, Cambridge CB2 1EC, UK. Fax: int. Code + 44(0) 1223/336-033. E-mail: deposit@chemcrys.cam.ac.uk.

3 even reacts with an aqueous solution of nPen$_4$NBr to afford the likewise sparingly soluble, new assembly [(nPen$_4$N)(Me$_3$Sn)$_2$Ir(CN)$_6 \cdot x$H$_2$O] (**3c**). From the mother liquors resulting after filtration, single crystals suitable for a crystal structure analysis could so far only be obtained in the case of **3a**. As another representative containing the nPr$_4$P$^+$ ion, the new product **1a-P** (M = Co) was likewise prepared. Here, single crystals could again be obtained from the mother liquor within a few days. The chemical compositions of **1a-P**, **3a**, **3a-P**, **3b**, and **3c** could be established by combining independent results from elemental analysis and ^{1}H NMR spectroscopy in D$_2$O/NaOD solution. The latter, quite elegant technique allows the independent determination of the respective R_4E/Me$_3$Sn ratios (7, 8). According to its elemental analysis, **3c** seems to be richer in H$_2$O ($m \geq 2$) than **1c** and **2c** (8).

In spite of its notably lower solubility in H$_2$O as compared with **1**, its slightly modified derivative **4** (9) reacts almost quantitatively with nPr$_4$NCl to **4a**. In contrast, the corresponding reaction with nBu$_4$NCl (over about 20 h) had afforded only a product with the unsatisfactory (for pure **4b**) nBu$_4$N/Co(CN)$_6$ ratio of ca. 0.6 (14). However, we succeeded in preparing the desired product **4a** = [(nBu$_4$N){Me$_2$Sn(CH$_2$)$_3$SnMe$_2$}Co(CN)$_6 \cdot$ 2H$_2$O] readily by co-precipitation.

The infrared (IR) spectra of all R_4N-containing assemblies display, inter alia, notably more intense ν(CH) bands than the spectra of **1** and **3**. Surprisingly few ν(CN) bands are, however, found (see Experimental section), in spite of the rather low local symmetry of the immediate surroundings of the M(CN)$_6$ fragments (*vide infra*). The vibrational frequencies adopt values intermediate between those of **1** and **3** (involving M–CN → Sn bridges) and of K$_3$[M(CN)$_6$] (M = Co or Ir), respectively (with terminal CN ligands only). Interestingly, all initially colorless R_4N-containing assemblies with M = Co(III) convert at ca. 300°C into blue products, involving presumably Co(II). For M = Ir, less pronounced color changes toward yellow occur.

X-ray Powder Diffractometric (XRD) Studies

All the new supramolecular assemblies studied except **4b** and **1a-P** gave rise to satisfactory XRDs with numerous pronounced and sharp reflections. The experimental XRD of **3a** resembles strongly its simulated diffraction pattern (Fig. 1), based upon data of the successful single-crystal X-ray study of this compound (*vide infra*). This excellent coincidence qualifies the polycrystalline (bulk) material of **3a** also for a promising CP MAS solid-state NMR study in taking here the crystallographically determined asymmetric unit fully for granted. According to Fig. 1, the XRDs of **3a** resemble, moreover, those of **1a** (8) (Fig. 1). **3a** is in fact found to be practically isostructural with **1a** (*vide infra*).

Figure 2 reveals that the experimental XRD of **1a-P** resembles only faintly that of co-precipitated **1a**, although notably better agreement is found for the two *simulated* XRDs. Although the latter findings reflect the fact that **1a-P** and **1a** *are* actually isostructural (*vide infra*), the experimental XRDs of both compounds indicate some deficiencies for the bulk samples. We have shown earlier (8) that some "amendment" of the simulated XRD of co-precipitated **1a** is in principle possible, provided that e.g. a preferred orientation of the crystallites in the bulk material can be accounted for.

In Fig. 3 the experimental XRDs of **3b** (R = nBu) and **3c** (R = nPen) are compared with the simulated XRDs of **2b** (7) and **2c** (8). While there seems to be hardly any similarity of the diffraction patterns of **3b** and **2b** and of **3c** and **2c**, respectively, the pattern of **3b** resembles somewhat more that of **3a** (see Fig. 1). It would, however, be premature to draw here any more distinct conclusion. In view of the excellent quality of the XRD of bulk **3b**, this sample may be expected to be a promising candidate for multinuclear CP MAS solid-state NMR studies. The multinuclear solid-state NMR spectra of diamagnetic **1b**, which have already been investigated in great detail (7), could offer helpful guidelines for a structure-oriented NMR study of **3b** (*vide infra*).

In Fig. 4 the experimental XRD of co-precipitated **4a** is compared with the simulated XRDs of **3a** and **1a** (8). During this simulation of the XRD of **3a**, all positions of Ir atoms were also replaced by the lighter Co atoms. In principle, all three diffractograms resemble each other, suggesting for **4a** a crystal structure similar to those found for **1a** (8) and **3a** (*vide infra*). Although the trimethylene tether of **4a**, which holds its Me$_2$Sn units pairwise together, must be considered as an additional structure-directing factor, the comparatively "light" additional CH$_2$ and CH$_3$ fragments present in derivatives of **4** are, according to a Rietveld analysis of the host/guest system [(Et$_4$N)(Me$_3$Sn)$_3$Fe(CN)$_6$] (15), unlikely to generate pronounced, additional reflections. A closer inspection of the three XRDs depicted in Fig. 4 appears to reveal a slightly closer similarity of **4a** with (modified) **3a** than with **1a**, the diffractogram of which was still simulated for the initially evaluated space group $P2_12_12$ (8). However, according to our crystallographic results for **3a** (*vide infra*), this space group might be abandoned in favor of $P2_12_12_1$. Finally, a comparison of the experimental XRD of **4b** with the simulated diffractogram of **1b** (7) (Fig. 5) reveals immediately that, probably owing to the presence of the trimethylene tether, the rather complicated supramolecular architecture of **1b** and **2b** cannot be realized in **4b**. Thus, **2b** contains three *chemically* nonequivalent Me$_3$Sn fragments in distinct positions of the lattice (7).

*Crystal Structures of **3a** and **1a-P***

The results of the crystallographic studies of single crystals of **3a** and **1a-P** confirm our earlier findings (8),

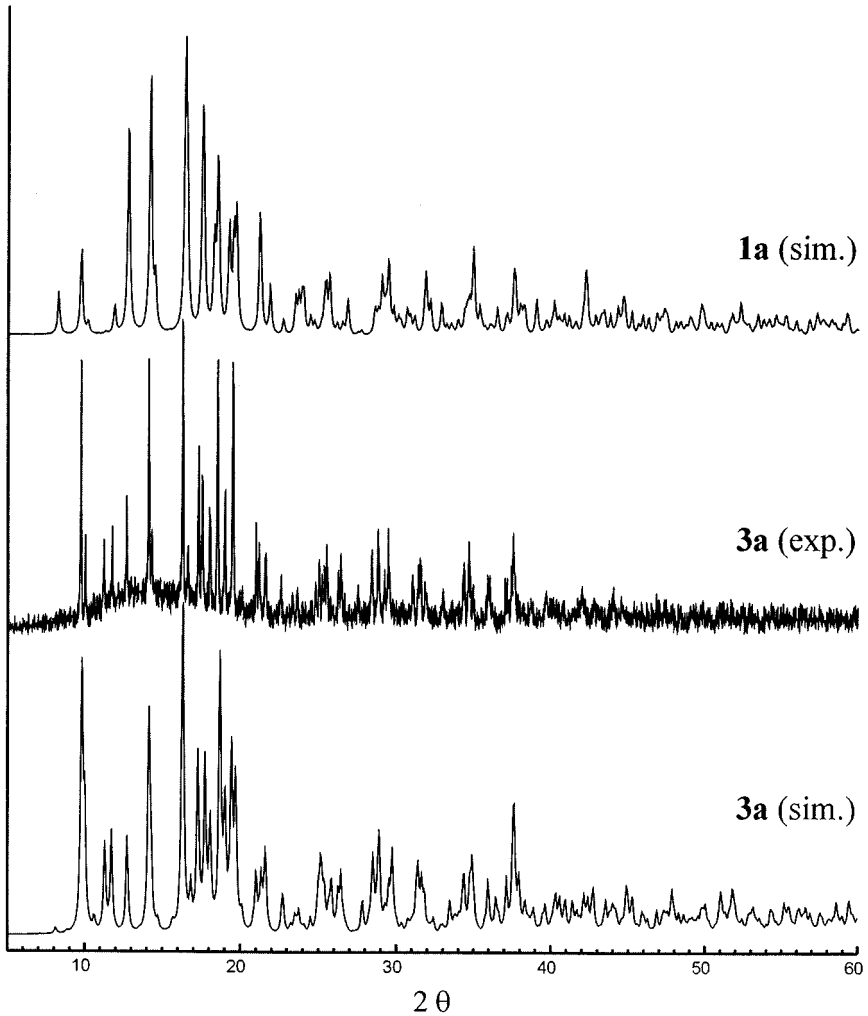

FIG. 1. Comparison of the experimental (b) and simulated (c) XRDs of **3a** with the simulated XRD of **1a** (a).

according to which in the presence of R_4E^+ ions with $R = n$-propyl the primary building blocks Me_3Sn^+, $[M(CN)_6]^{3-}$, and H_2O afford negatively charged *molecular* units of the type $[M(CN)_4(CNSnMe_3 \cdot OH_2)_2]^-$, which assemble to infinite frameworks exclusively via O–H ⋯ NC hydrogen bonds. The resulting 2-D or 3-D frameworks incorporate the $n Pr_4E^+$ guest ions quite specifically. While **3a** contains, like **1a** (8), anionic metal complexes with two *cis*-configured $CNSn(Me_3)OH_2$ ligands per iridium center, **1a-P** represents, like (co-precipitated) **1a** (8), the corresponding trans-isomer with $M = Co$ (Figs. 6 and 7).

Relevant crystal and refinement parameters of **3a** and **1a-P** are collected in Table 1, and selected interatomic distances and bond angles, respectively, of **3a** and **1a-P** are listed in Tables 2 and 3. In contrast to numerous other host/guest systems containing R_4N^+ ions (4,5), the $n Pr_4E^+$ guests of **3a** and **1a-P** are not disordered. The asymmetric units of **3a** and **1a-P** are shown in Figs. 6a and 7a.

The $\{Ir(CNSn(Me_3)OH_2)_2\}$ fragment of **3a** is, like that of its cobalt homologue **1a** (8), V-shaped (C1–Ir–C2 angle: 88.12(19)°). However, while the methyl groups of the fragment with $M = Co$ were found to be disordered (8), a corresponding disorder can strictly be ruled out for $M = Ir$ (**3a**). Only the rotational ellipsoids of the three methyl carbon atoms of Sn2 turn out to be somewhat more expanded than those of Sn1 (Fig. 6a), which feature might reflect some faint disposal for disorder. All tin-bonded methyl carbon atoms of **3a** are bent almost negligibly toward the oxygen atom, while for **1a** more pronounced bending toward the oxygen *and* the nitrogen atoms, respectively, was observed. Interestingly, the solid-state NMR results reported for the ^{119}Sn and methyl ^{13}C nuclei of **1a** (8) would be fully consistent with the asymmetric unit of **3a**, but not with that of **1a**. In view of this fact, the validity of the space group $P2_12_12_1$ also for compound **1a** should no longer be ruled out, in spite of the absence of several appropriate reflections (8).

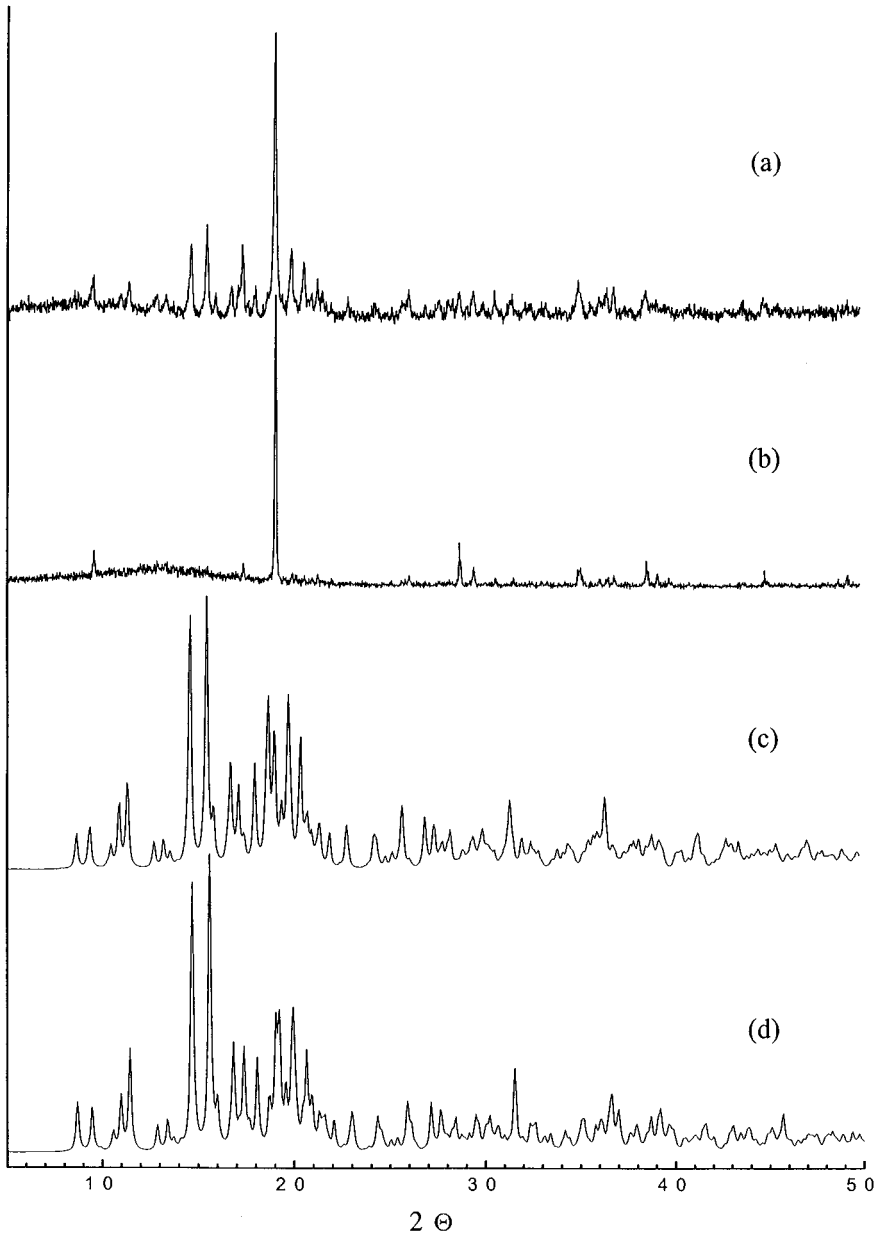

FIG. 2. Comparison of the experimental XRDs of co-precipitated **1a** (a) and **1a-P** (b) with the simulated XRDs of **1a-P** (c) and co-precipitated **1a** (d), respectively.

O–H ··· NC hydrogen bonds corresponding to those found for **1a** (8), both as far as the O ··· N distances and the actual number of these interactions (per formula unit) are concerned (Table 2), interlink all *cis*-$[Ir(CN)_4(CNSnMe_3OH_2)_2]^-$ anions to infinite, puckered layers between which the nPr_4N^+ guest ions are incorporated (Fig. 6b). Interestingly, the three shortest C ··· N distances of **3a** originate from α-CH_2 groups of the guest cation and likely reflect C–H ··· NC hydrogen bonds (Table 2). However, in length they exceed the shortest C ··· N contacts of **1a** (3.13–3.17 Å) (8) considerably. Nevertheless, the nPr_4N^+ cation of **3a** is, in contrast to that of **1a**, not disordered.

The *trans*-$[Co(CN)_4(CNSnMe_3 \cdot OH_2)_2]^-$ ions of **1a-P** and co-precipitated **1a** (8) are even more similar in shape, and also in their metrical parameters (Table 3), than the corresponding *cis*-configured anions of **3a** and **1a** (*vide supra*). As in the structure of co-precipitated **1a**, the only disordered non-hydrogen atom of **1a-P** is O1, which belongs to one of the two Sn-coordinated water molecules. As

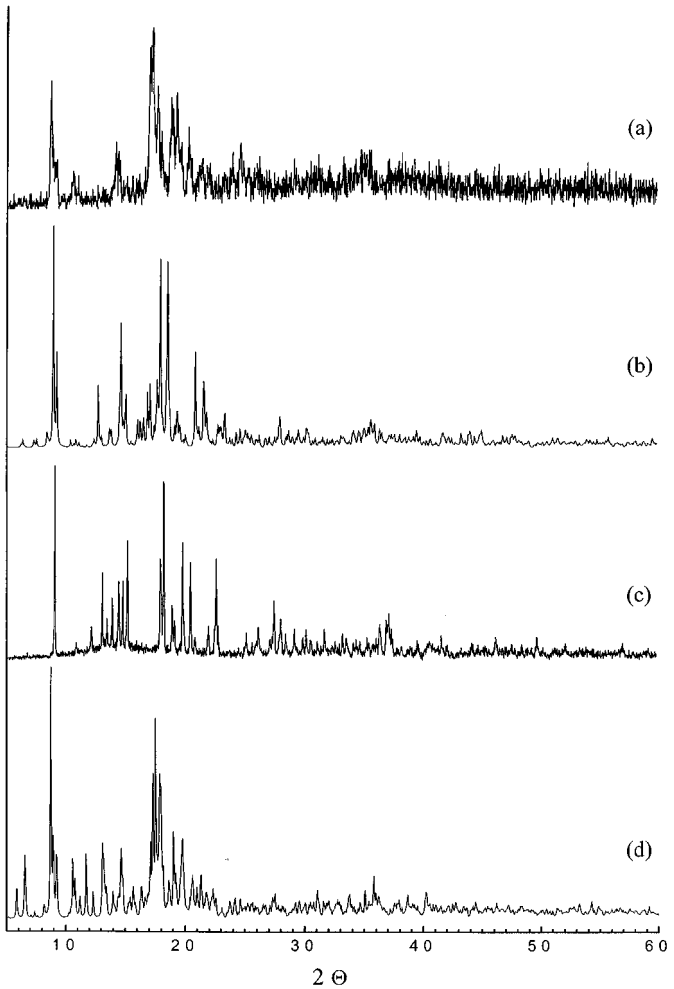

FIG. 3. Comparison of the experimental XRDs of **3b** (c) and **3c** (a) with the already reported (8), simulated XRDs of **2b** (d) and **2c** (b).

in **3a**, all four virtually terminal cyanide ligands of **1a-P** are involved in O–H ··· NC hydrogen bonds with O ··· N distances between 2.689 and 2.754 Å (Table 3). Owing to three of the four hydrogen bonds to be expected per formula unit, well-ordered, puckered *layers* result. These layers are, moreover, held together by the fourth hydrogen bond (i.e., O2–H ··· N3), affording thus a veritable 3-D framework (Fig. 7b). The disorder of the oxygen atoms O1 and O3, which is observed both for **1a-P** and co-precipitated **1a**, might be essential to guarantee optimal intralayer hydrogen bonding with all of the otherwise terminal cyanide ligands. The $n\mathrm{Pr}_4\mathrm{P}^+$ guest ions are encapsulated between adjacent layers. Less conventional are notably weaker C–H ··· N hydrogen bonds that are, again, likely to be responsible for the lack of any disorder of the organic cation, although the shortest C ··· N distances found for **1a-P** exceed 3.40 Å (Table 3). At least two of the α-CH_2 groups of the $n\mathrm{Pr}_4\mathrm{P}^+$ ion could be weakly anchored to cyanide N atoms. A closer comparison of the relevant C ··· N distances of **1a-P** with those of **1a** (8) suggests that the intraframework fixation of the $n\mathrm{Pr}_4\mathrm{P}^+$ ion resembles that of the $n\mathrm{Pr}_4\mathrm{N}^+$ ion (in co-precipitated **1a**). Up to now, very little is known about "unconventional" C–H ··· *X* hydrogen bonds involving $R_4\mathrm{P}^+$ instead of $R_4\mathrm{N}^+$ ions as a C–H source (16). According to a recent evaluation by Desiraju *et al.* (17), at least C–H ··· N hydrogen bonds with C ··· N distances of up to 3.75 Å may in fact be of relevance for the generation of supramolecular assemblies (provided that the H atom belongs to an aromatic hydrocarbon). On the other hand, C–H ··· O hydrogen bonds as short as 3.2 Å (C ··· O) have most recently been suspected to foster protein folding (18).

*3.4. Multinuclear (^{13}C, ^{31}P, ^{119}Sn) Solid-State Magnetic Resonance Spectra of **1a-P**, **3a**, **3b**, **3a-P**, and **4a***

Important information regarding structural features can also be deduced from the CPMAS ^{119}Sn NMR spectra (Fig. 8). Including sideband distributions, the ^{119}Sn spectra of the iridium systems containing propylammonium and -phosphonium cations (**3a** and **3a-P)** are very similar and resemble, moreover, the already reported spectrum (8) of the

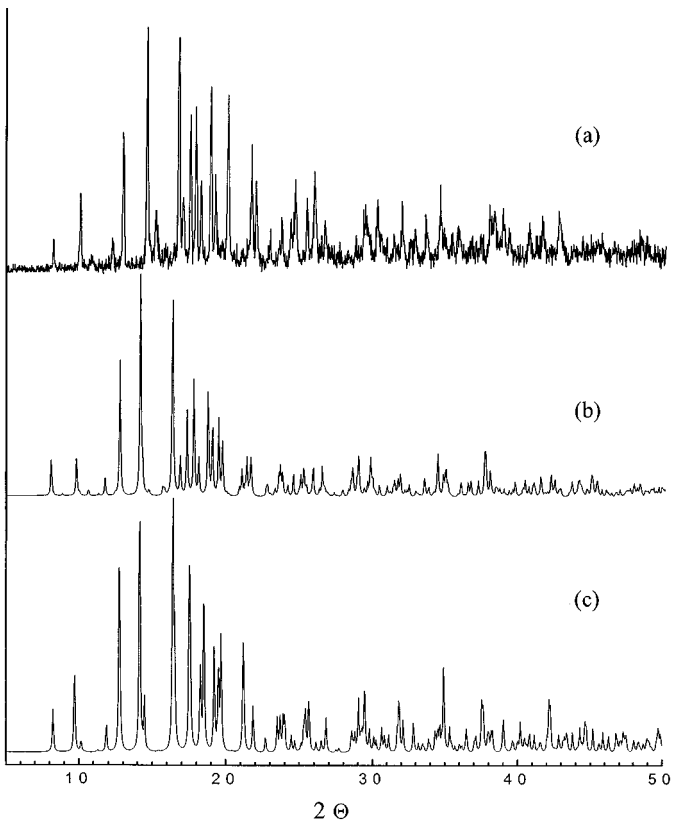

FIG. 4. Comparison of the experimental XRD of **4a** (obtained by co-precipitation; top) with the simulated XRDs of **3a** (b) and **1a** (c). Curve (b) was calculated for M = Co (see the text).

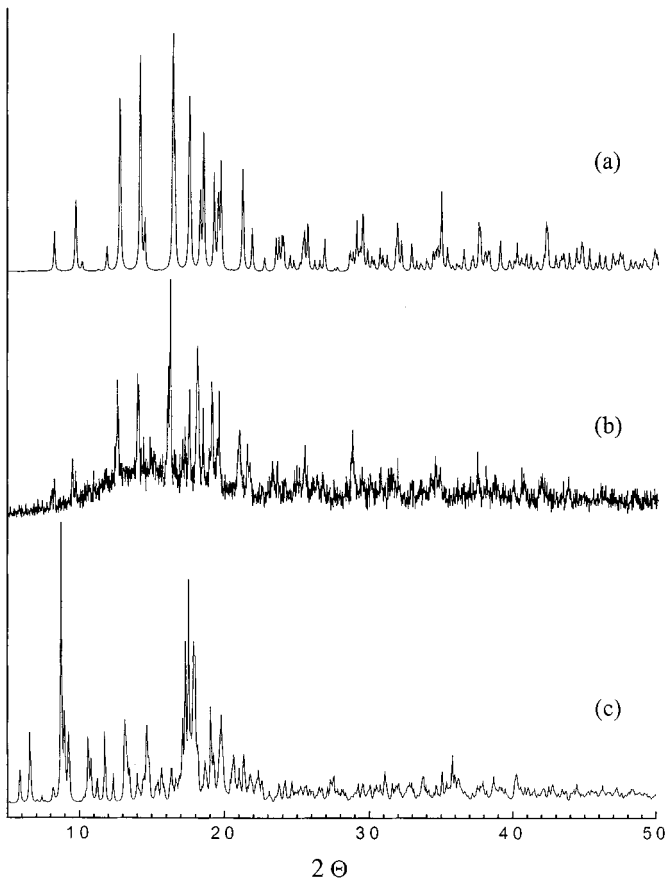

FIG. 5. Comparison of the experimental XRD of **4b** (obtained by co-precipitation; b) with the simulated XRDs of **1a** (a) and **2b** (c).

cobalt analogue **1a**. The spectrum of **1a** looks also like that of its derivative **4a**, wherein tin atoms are held together pairwise by trimethylene tethers. All these four compounds display *two* centerbands (between -60 and -80 ppm), with isotropic chemical shifts characteristic of trigonal bipyramidal $\{CNSn(Me_3)OH_2\}$ fragments (7) best attributable to the two nonequivalent, cis-oriented $CNSnR_3 \cdot OH_2$ ligands of a Co^{3+} (**1a**, **4a**) or an Ir^{3+} (**3a**, **3a-P**) ion. For **1a** (8) and **3a** (*vide supra*), this arrangement has been confirmed by X-ray crystallography. The two centerbands of **1a** were resolved into multiplets, giving rise to two *different* coupling parameters $|J^{119}Sn, {}^{14}N|$ and, in the case of ^{15}N-enrichment, to two *different* $|J^{119}Sn, {}^{15}N|$ values (8). In the other cases the somewhat larger line widths (380–580 Hz) may obscure such a fine structure. While, from its X-ray study (8), the Me_3Sn groups of **1a** were found to be apparently crystallographically equivalent, but nevertheless disordered, those of **3a** (and probably of **3a-P**, too) are definitely nonequivalent, but undoubtedly devoid of any disorder. Of course, the NMR information makes it quite clear that there are actually nonequivalent Me_3Sn groups in **1a** also. Taking for granted that the Me_3Sn units of **1a** are just disordered in the two environments, the similarity of all *four* compounds in their ^{119}Sn shifts (Table 4) is somewhat surprising.

The ^{119}Sn spectrum of the iridium compound containing tetrabutylammonium cations (**3b**; Fig. 8b**)** differs notably from that of its cobalt homologue **1b** (Fig. 8a, top), which contains up to five centerbands at very different chemical shifts (7). In contrast, the spectrum of **3b** resembles those of **1a**, **3a**, and **3a-P**, but with a significantly smaller chemical shift difference between the two tin sites. These findings support the doubts about an isostructural architecture of **3b** on the one hand and of **1b** and **2b** on the other, which have already been suggested in view of the XRD of **3b** (*vide supra*).

The ^{119}Sn spectrum of the cobalt compound containing Pr_4P^+ cations (**1a-P)** resembles strongly that of *co-precipitated* **1a** (8). According to single-crystal X-ray crystallography, these two solids are in fact isostructural and involve two nonequivalent, trans-configured $CNSnMe_3 \cdot OH_2$ ligands. Although the ^{119}Sn spectrum of **1a-P** exceeds that of **1a** in quality, again only one centerband appears. The isotropic chemical shift agrees with that expected for $CNSnMe_3OH_2$ fragments (**1a-P**: -78 ppm). The apparent absence of a second ^{119}Sn resonance (as required by the asymmetric unit; see Fig. 7) may arise from an accidental near-degeneracy. Alternatively, it may support the suggestion (8) that at room temperature rapid (on the NMR time scale) interchange of Sn1 and Sn2 (in each compound) might take place. In the case of co-precipitated **1a**, only one ^{15}N cyanide signal was detected instead of the six expected lines. Actually, *six* crystallographically nonequivalent N atoms were found in the asymmetric units of both **1a-P** and **1a** (8). Moreover, the modest quality of the XRDs of bulk **1a-P** and co-precipitated **1a** (Fig. 2) might also reflect some NMR-relevant deficiencies of the samples.

According to the literature (19), an unstrained trimethylene bridge connecting two tin atoms requires a Sn ··· Sn separation of about 6.15 Å. A systematic examination of the crystal structures of **3a** and **1a-P** in view of such Sn ··· Sn distances reveals that the most favorable location for the $(CH_2)_3$ tether would be *within* each $\{cis\text{-}M(CN)_4(CNSnMe_3 \cdot OH_2)_2\}$ fragment of **3a**, according to Fig. 9. *Inter*-fragment tethering would, in principle, also be possible within the crystal lattices of **1a-P** and **3a**, but only if accompanied by some more constraint. The appearance of *two* ^{119}Sn centerbands for **4a** indicates a non-negligible lack of symmetry for the tether, which might just reflect the inequivalence of the two cis-oriented $CNSnR_3 \cdot OH_2$ ligands. The ^{119}Sn shielding tensor parameters obtained by spinning sideband analysis of the spectra for **1a-P**, **3a**, **3a-P**, **3b**, and **4a** are very consistent. The anisotropies range between -309 and -347 ppm and the asymmetries lie around 0.1 (except for **4a**, which has somewhat higher values), implying zero within experimental error.

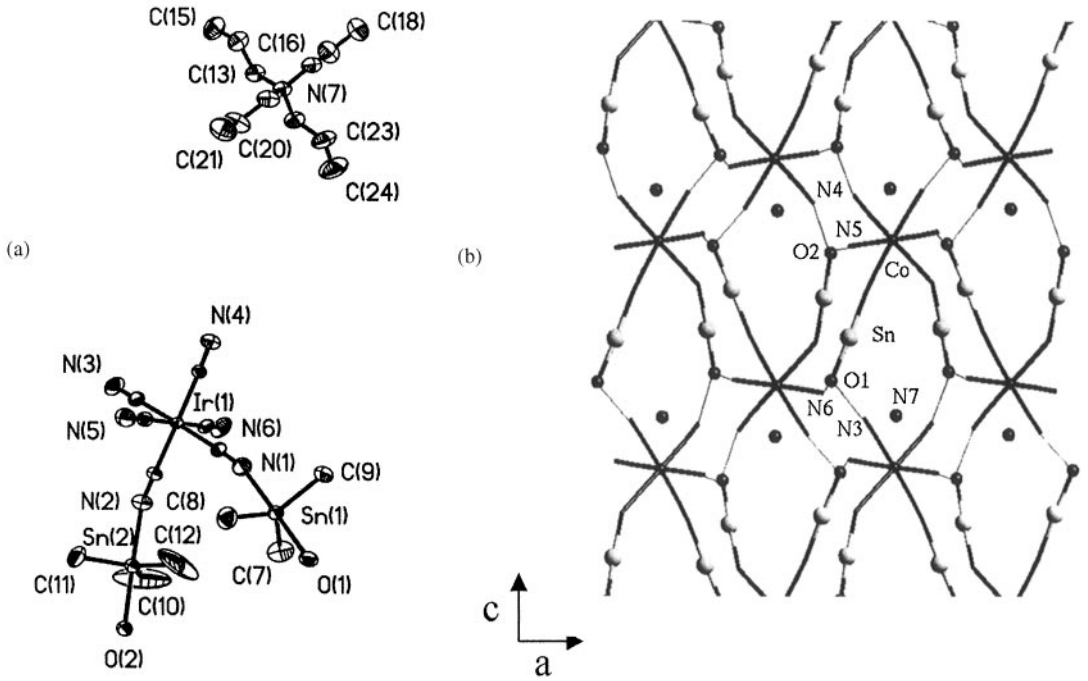

FIG. 6. Asymmetric unit (a) and supramolecular architecture (b) of **3a**. Faint lines symbolize O–H ··· N ≡ C hydrogen bonds, larger grayish spheres representing tin atoms (methyl groups have been omitted). N7 is the center of a $n\mathrm{Pr_4N^+}$ ion.

While the ^{31}P NMR spectra of **1a-P** and **3a-P** show just one singlet each (see footnote *a* of Table 4), in accordance with the asymmetric unit of the former, the ^{13}C spectra (see Fig. 10) are unusual in that the *n*-propyl resonances of the latter sample give rise to just one broad signal at 17 ppm, with a low-frequency shoulder, whereas for **1a-P** two separate, but likewise broad, bands appear (the crystallographic nonequivalence of the four alkyl groups not giving any definitive extra splitting). Moreover, instead of the two expected methyl carbon resonances (of the two different, rapidly rotating Me_3Sn groups), only one extremely weak signal appears in the spectrum of **1a-P** at a chemical shift of around 1 ppm (along with one slightly stronger peak at 6 ppm). In the ^{13}C spectrum of $n\mathrm{Pr_4PBr}$ dissolved in D_2O, two ^{13}C doublets (α- and β-CH_2) and one singlet (γ-CH_3) occur between 22 and 14 ppm (see Table 4). Nagy *et al.* (20) have compared the ^{13}C NMR spectra of $n\mathrm{Bu_4P^+}$ and $n\mathrm{Bu_4N^+}$ ions present in as-prepared zeolites ZSM-11, but corresponding solids containing $n\mathrm{Pr_4N^+}$ or $n\mathrm{Pr_4P^+}$ ions have so far not been considered. The ^{13}C NMR spectrum of the Ir-containing homologue **3a-P** of **1a-P** displays two pronounced singlets close to 2 ppm (corresponding to two rotating Me_3Sn groups), and there are two or three signals between 100 and 115 ppm (cyanide carbons). In contrast to **1a-P**, the ^{13}C spectrum of the $n\mathrm{Pr_4N^+}$-containing homologue **3a** of **3a-P** behaves in a more regular fashion in that sufficiently intense resonances appear for *all* four different types of carbon atom present in this assembly. Again, two methyl singlets indicate the presence of two different, rapidly rotating Me_3Sn groups, while in disagreement with the asymmetric unit, only one α-CH_2 singlet and one β-CH_2 singlet appear (though in both cases the lines are broad). However, the corresponding γ-CH_3 singlet carries a weak shoulder. A complex series of signals appears in the cyanide carbon range.

The ^{13}C spectrum of compound **4a**, which contains a trimethylene tether between each pair of tin atoms, displays in principle all of the resonances expected (Table 4). The three quasi-singlets found around zero ppm (the central one of which is about twice as intense as the two others and may have an incipient splitting) must be ascribed to the four nonequivalent, rigidly tin-bonded methyl groups. According to our earlier findings (9), the broad signal centered at 23.3 ppm is most likely due to the three carbon atoms of the trimethylene tether. The remaining signal groups may then, in close analogy to those of e.g. **3a**, be readily assigned to the α-, β-, and γ-carbon atoms of the *n*-propyl units, with some clear splitting of the γ resonance.

The ^{13}C spectrum of compound **3b** confirms the suggestion that this assembly cannot be isostructural with **2b** and **1b** (*vide supra*) as its resonances for the tin-bonded methyl groups differ significantly from those of **1b**. In contrast, this resonance pattern of **3b** resembles strongly those of **3a** and **3a-P**. The remaining part of the ^{13}C spectrum of **3b** (except that for the cyanide carbons) seems to reflect one comparatively "tightly" anchored $n\mathrm{Bu_4N^+}$ ion with four

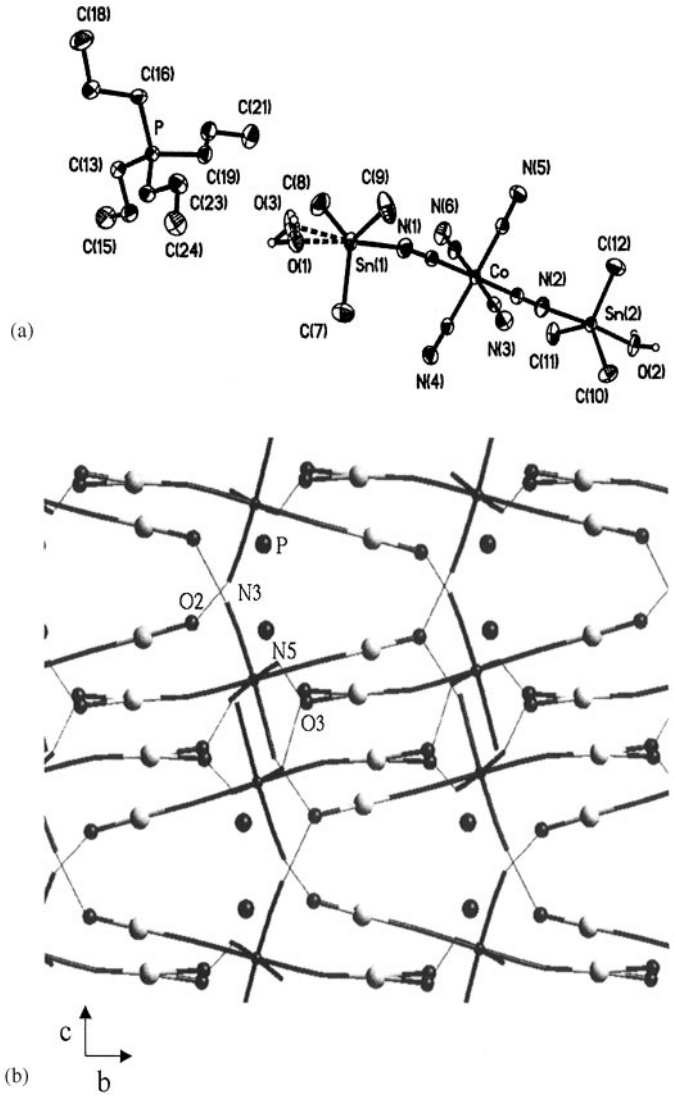

FIG. 7. Asymmetric unit (a) and supramolecular architecture (b) of **1a-P**. For further explanations see the legend of Fig. 6.

crystallographically nonequivalent butyl groups as approximately four individual signals may be detected for the α-, β-, γ-, and δ-carbon atoms, respectively (counting two notably intense signals twice). Precise assignment of the β-, γ-, and δ-resonances is difficult, however. Reports on ^{13}C CPMAS NMR studies of as-prepared zeolites with $n Pr_4N^+$ guests are still rather scarce. Interestingly, the $n Pr_4N^+$ ions occluded in SAPO-40 are reported to display *more* signals at 373 K than at 297 K (21).

CONCLUSIONS

The solid-state NMR results (in particular for the nuclei ^{119}Sn and ^{31}P) complement the X-ray diffraction results in that (a) throughout the presence of just one singular species per bulk sample is indicated. (b) The absence of ^{119}Sn centerbands for $\delta < -90$ ppm (as typical for $\{trans\text{-}Me_3Sn(NC)_2\}$ fragments) strongly suggests that all samples studied here are devoid of ⫞M–CN–Sn–NC⫟ chains. Thus, even the $n Bu_4N^+$ ion seems to initiate a total cleavage of the 3-D framework of **3**, although **1** and **2** are reported to withstand a cleavage by this ion at least partially (7). (c) Representatives of type **1a** and **3a**, respectively, with two either cis- or trans-oriented $CNSn(Me_3)OH_2$ ligands may readily be distinguished by their ^{119}Sn spectra. (d) The striking similarly of the NMR spectra of **1a** and **3a** suggests that the structure analysis of the former is probably based upon an incomplete manifold of reflections. (e) All NMR results for **4a** (including those for ^{13}C) favor the view that this assembly is also isostructural with **3a**, involving again two cis-oriented and $(CH_2)_3$-interlinked $CNSn(R_3)OH_2$ ligands. (f) Bulk samples displaying unsatisfactory XRDs also tend to yield more truncated NMR results (e.g., **1a-P** and co-precipitated **1a**). A reverse situation holds e.g. for **3b**.

The results described in the present contribution thus confirm, and generalize, our earlier findings (8), according to which $n Pr_4N^+$ ions will behave as "efficient" cleaving agents of Me_3Sn-containing *super*-Prussian blue systems, and are even capable of generating two isomers of the composition $[(Pr_4N)(Me_3Sn)_2M(CN)_6 \cdot 2H_2O]$ devoid of any [*M*–CN–Sn–NC] *chains*. In contrast, assemblies of the different types $[(R_4E)_x(Me_3Sn)_{4-x}Fe^{II}(CN)_6 \cdot yH_2O]$ with $R = n Pr$ have been found to differ significantly in their *stoichiometry* for $E = N$ ($x \approx 1.0$) and $E = P$ ($x \approx 0.47$), respectively (22).

Replacement of Co by Ir in the $[M(CN)_6]^{3-}$ building block leads to generally isostructural, but less insoluble, homologues, implying on the other hand the advantage that single crystals suitable for X-ray studies are more readily accessible. As the $[Ir(CN)_6]^{3-}$ ion seems to afford, *un*like its $[Co(CN)_6]^{3-}$ homologue, structurally quite similar assemblies with both $n Pr_4E^+$ and $n Bu_4N^+$ ions, only the combination of the building blocks $[Co(CN)_6]^{3-}$, $\{Me_3Sn\}^+$, and H_2O (1 : 3 : 2) leads at present to the structurally most versatile manifold of supramolecular assemblies. This interesting feature may be compared with "supramolecular recognition" in its commonly understood meaning.

It is also remarkable that even compound **4** is readily "attacked" by the $n Pr_4N^+$ ion, although **4** is notably more insoluble than **1**. As one formula unit of **4a** is poorer than **4** in one-half of a $\{Me_2Sn(CH_2)_3SnMe_2\}^{2+}$ unit, aqueous suspensions of **4** must still be assumed to equilibrate with various solvated dissociation products, including also the "bidentate" $\{Me_2Sn(CH_2)_3SnMe_2\}^{2+}$ ions (23). On the other hand, compound **4b** could only be prepared by co-precipitation (*vide supra*), most probably owing to the limited $\{Me_2Sn(CH_2)_3SnMe_2\}^{2+}$ concentration in equilibrium with **4**.

TABLE 1
Crystallographic Parameters of 1a-P and 3a

	1a-P	3a
Empirical formula	$C_{24}H_{50}N_6O_2PCoSn_2$	$C_{24}H_{50}N_7O_2IrSn_2$
Formula weight	781.98	898.29
Crystal system	Orthorhombic	Orthorhombic
a (Å)	18.811	11.2369(2)
b (Å)	18.9278(2)	15.07290(10)
c (Å)	20.3692(2)	21.8015(2)
V (Å^3)	7252.47(10)	3692.58(8)
Z	8	4
Space group	*Pbca*	$P2_12_12_1$
T (K)	173(2)	173(2)
λ (Mo$K\alpha$) (Å)	0.71073	0.71073
ρ_{calc} (g cm^{-3})	1.427	1.609
μ (mm^{-1})	1.889	4.964
F (000)	3128	1728
Crystal size (mm)	$0.6 \times 0.5 \times 0.4$	$0.7 \times 0.5 \times 0.3$
θ range of data collection (°)	1.82–29.19	1.64–29.51
Index ranges	$-25 < h < 15,\ -18 < k < 25,\ -24 < l < 27$	$-13 < h < 15,\ -20 < k < 17,\ -22 < l < 30$
No. of reflcns. collected	47,583	25,512
No. of indep. reflcns.	9508 [R(int) = 0.0284]	9597 [R(int) = 0.0411]
No. of obsd. reflcns. [$I > 2\sigma(I)$]	8396	8837
No. of data/restraints/parameters	9508/0/364	9597/0/339
Goodness-of-fit on F^2	1.103	0.899
R indices [$I > 2\sigma(I)$]	$R1 = 0.0226$, w$R2 = 0.0511$	$R1 = 0.0287$, w$R2 = 0.0668$
R indices (all data)	$R1 = 0.0293$, w$R2 = 0.0539$	$R1 = 0.0321$, w$R2 = 0.0683$
Largest diff. peak and hole (eÅ^{-3})	1.422 and −0.730	2.033 and −1.952

Note. $w = l/[s^2(F^2) + (xP)^2 + yP]$ where $P = (F_o^2 + 2F_c^2)/3$; **1a-P** ($x = 0.0180$, $y = 5.2693$); **3a** ($x = 0.0275$, $y = 0.000$).

TABLE 2
Selected Interatomic Distances (Å) and Angles (°) of 3a (Dotted Lines Refer to Potential O–H ⋯ N and C–H ⋯ N Hydrogen Bonds, Respectively, Considering Here Only C ⋯ N Distances < 3.80 Å)

Sn1–N1	2.332(5)	Sn1–C7	2.123(5)
Sn2–N2	2.347(5)	Sn1–C8	2.123(6)
Sn1–O1	2.286(3)	Sn1–C9	2.120(6)
Sn2–O2	2.275(3)		
		Sn2–C10	2.076(9)
O1 ⋯ N3	2.647(6)	Sn2–C11	2.055(8)
O1 ⋯ N6	2.6689(7)	Sn2–C12	2.095(8)
O2 ⋯ N4	2.776(5)		
O2 ⋯ N5	2.715(6)	C16 ⋯ N3	3.532(7)
		C22 ⋯ N5	3.555(8)
Sn1–N1–C1	164.6(4)	C13 ⋯ N5	3.603(8)
Sn2–N2–C2	151.4(4)	C20 ⋯ N4	3.691(8)
N1–Sn1–O1	177.08(16)		
N2–Sn2–O2	177.69(15)	N1–Sn1C7	94.1(2)
		N1–Sn1–C8	90.9(2)
Sn1–O1 ⋯ N3	108.88(17)	N1–Sn1–C9	91.9(2)
Sn1–O1 ⋯ N6	113.67(19)	N2–Sn2–C10	90.8(3)
Sn2–O2 ⋯ N4	128.0(2)	N2–Sn2–C11	91.6(3)
Sn2–O2 ⋯ N5	117.53(18)	N2–Sn2–C12	89.0(3)

TABLE 3
Selected Interatomic Distances (Å) and Angles (°) of 1a-P (Dotted Lines Refer to Potential O–H ⋯ N and C–H ⋯ N Hydrogen Bonds, Respectively, Considering Here Only C ⋯ N Distances < 3.80 Å)

Sn1–N1	2.2988(17)	Sn1–C7	2.120(2)
Sn2–N2	2.3444(17)	Sn1–C8	2.111(2)
Sn1–O1	2.291(10)	Sn1–C9	2.109(2)
Sn1–O3	2.293(10)	Sn2–C10	2.118(2)
Sn2–O2	2.2775(15)	Sn2–C11	2.120(2)
		Sn2–C12	2.125(2)
O1 ⋯ N4	2.777(9)		
O1 ⋯ N5	2.777(9)	C22 ⋯ N4	3.404(3)[a]
O3 ⋯ N4	2.733(10)	C14 ⋯ N3	3.433(3)
O3 ⋯ N5	2.751(10)	C13 ⋯ N5	3.435(3)[a]
O2 ⋯ N3	2.750(2)	C23 ⋯ N4	3.500(3)
O2 ⋯ N6	2.698(3)	C16 ⋯ N3	3.516(3)[a]
		C15 ⋯ N3	3.540(3)
Sn1–N1–C1	167.50(17)	C19 ⋯ N4	3.630(3)[a]
Sn2–N2–C2	176.56(18)	C24 ⋯ N4	3.697(3)
N1–Sn1–O1	173.89(17)	C16 ⋯ N6	3.708(3)[a]
N1–Sn1–O3	172.7(2)	C24 ⋯ N5	3.709(3)
N2–Sn2–O2	175.34(7)		
		N1–Sn1–C7	91.45(9)
O1–H–H4	158(4)	N1–Sn1–C8	90.65(9)
O1–H–N5	167(3)	N1–Sn1–C9	91.52(9)
O3–H–N4	154(4)	N2–Sn2–C10	90.46(8)
O3–H–N5	158(3)	N2–Sn2–C11	90.43(8)
O2–H–N3	176(3)	N2–Sn2–C12	92.07(9)
O2–H–N6	162(4)		

[a] α-CH_2 group.

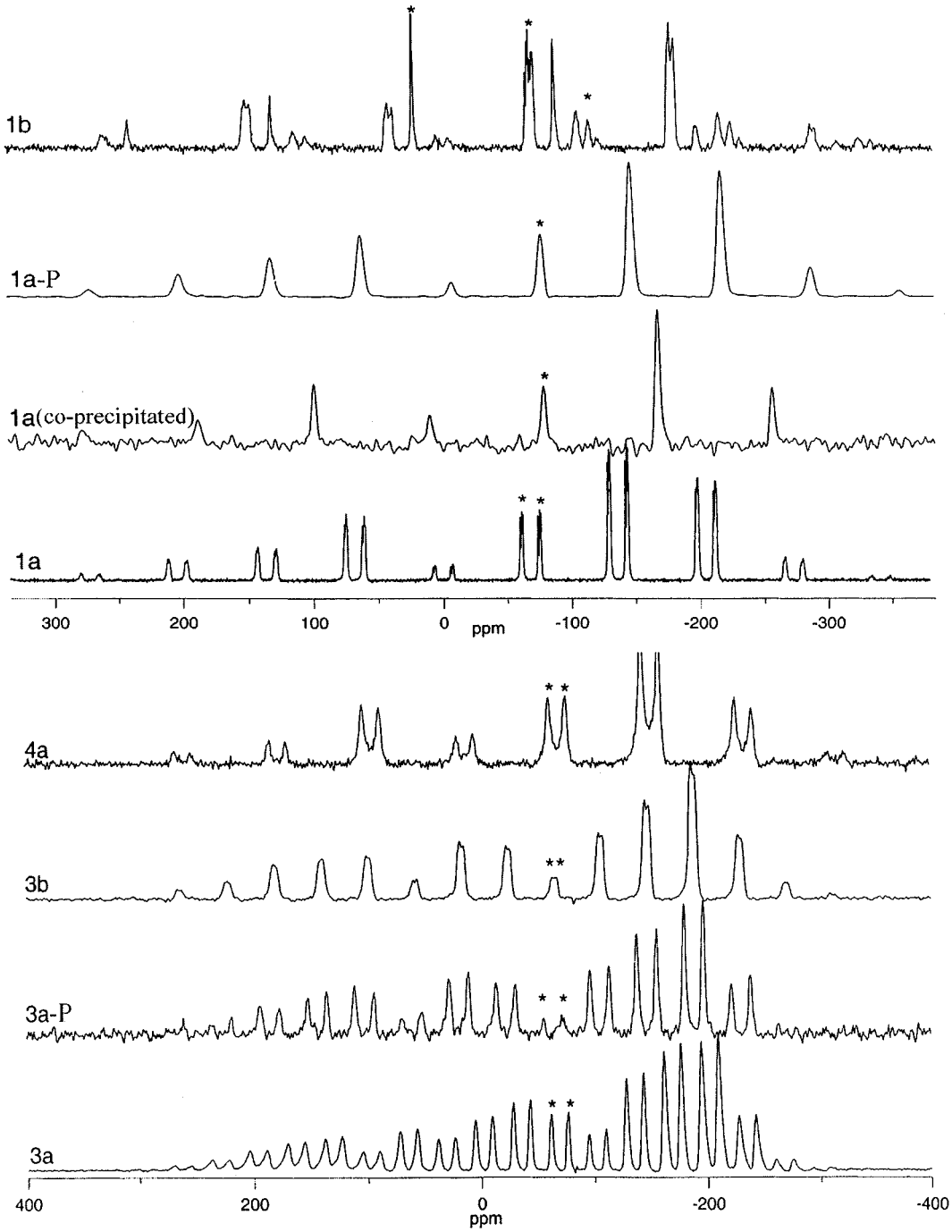

FIG. 8. ^{119}Sn CPMAS spectra (including spinning sideband distributions) of (a) **1a**, **1a** (by co-precipitation), **1a-P** and **1b**, and (b) **3a**, **3a-P**, **3b**, and **4**. Centerbands are shown by asterisks. All the spectra were recorded at 111.8 MHz and ambient probe temperature using cross-polarization from protons with flipback. Note that the chemical shift scale of part (a) differs from that of part (b). Conditions: (**1a**) Contact time, 10.0 ms; acquisition time, 20.0 ms; recycle delay, 5.0 s; spin rate, 7680 Hz; number of transients, 65,536. (**1a** (by co-precipitation)) Contact time, 1.0 ms; acquisition time, 20.0 ms; recycle delay, 5.0 s; spin rate, 9940 Hz; number of transients, 32,768. (**1a-P**) Contact time, 1.0 ms; acquisition time, 3.0 ms; recycle delay, 5.0 s; spin rate, 8240 Hz; number of transients, 8856. (**1b**) Contact time, 1.0 ms; acquisition time, 9.9 ms; recycle delay, 2.0 s; spin rate, 12,220 Hz; number of transients, 29,500. (**3a**) Contact time, 5.0 ms; acquisition time, 5.0 ms; recycle delay, 2.0 s; spin rate, 3760 Hz; number of transients, 2000. (**3a-P**) Contact time, 4.5 ms; acquisition time, 5.0 ms; recycle delay, 2.0 s; spin rate, 7700 Hz; number of transients, 31,744. (**3b**) Contact time, 5.0 ms; acquisition time, 5.0 ms; recycle delay, 2.0 s; spin rate, 5000 Hz; number of transients, 28,404. (**4a**) Contact time, 4.5 ms; acquisition time, 5.0 ms; recycle delay, 2.0 s; spin rate, 9220 Hz; number of transients, 384.

TABLE 4
NMR Parameters of the Compounds 1a, 1a (Co-precipitated), 1a-P, 1b, 3a, 3a-P 3b and 4a

Sample Shorthand/lit.	Me–Sn	^{13}C shifts R_4N/R_4P	CN	^{119}Sn shifts Me_3Sn[g]
$[(n-Pr_4N)(Me_3Sn)_2Co(CN)_6 \cdot 2H_2O]$ = **1a** (by co-precipitation) (8)	ca. 0.5	ca. 61 (α-CH_2) 16.5 (β-CH_2) 13.6, 12.4, 11.6, 11.0 (γ-CH_3)	ca. 130[b]	−79.0
$[(n-Pr_4N)(Me_3Sn)_2Co(CN)_6 \cdot 2H_2O]$ = **1a** (8)	2.2, 1.2	60.1 (α-CH_2) 15.8 (β-CH_2) 12.5, 11.5 (γ-CH_3)	ca. 130[b]	−61.0, −75.0
$[(n-Pr_4P)(Me_3Sn)_2Co(CN)_6 \cdot 2H_2O]$[a] = **1a-P**	1.2,[c] 5.5[c]	22.3 (α-CH_2) 16.4 (β-CH_2/γ-CH_3)	 ca. 130[b]	−77.0
$[(n-Bu_4N)(Me_3Sn)_2Co(CN)_6 \cdot 2H_2O]$ = **1b** (7)	1.9, 1.6,[d] 1.5, 1.4,[d] 0.7,[e] 0.0, −0.2	ca. 59[b] (α-CH_2) 24.9 (β-CH_2) ca. 20[b] (γ-CH_2) ca. 14[b] (δ-CH_3)	120 to 145 (Broad band)	21.5, Ranges: −66 to −73[b] −105 to −123[b]
$[(n-Pr_4N)(Me_3Sn)_2Ir(CN)_6 \cdot 2H_2O]$ = **3a**	1.8, 1.2	60.0 (α-CH_2) 15.9 (β-CH_2) 12.2, 11.2[d] (γ-CH_3)	ca. 100[b]	−61.6, −76.6
$[(n-Pr_4P)(Me_3Sn)_2Ir(CN)_6 \cdot 2H_2O]$[a] = **3a-P**	2.1, 1.6	17.0 (α-CH_2, 15.7[d] β-CH_2/γ-CH_3)	Range: 99 to 115	−56.0, −75.0
$[(n-Bu_4N)(Me_3Sn)_2Ir(CN)_6 \cdot mH_2O]$ = **3b**	2.1, 1.3	59.5, 58.6, 57.8 (α-CH_2) 24.8, 23.7, 22.6, 21.4, 20.4, 19.5, 19.1,[d] 16.4, 15.6, 12.9 (β/γ-CH_2, δ-CH_3)	Range: 100 to 112	−64.2, −67.8
$[(n-Pr_4N)\{Me_2Sn(CH_2)_3SnMe_2\}Co(CN)_6 \cdot 2H_2O]$ = **4a**	3.2, 0.6, −1.7, 23.3[f]	60.0 (α-CH_2) 16.3, 15.5[d] (β-CH_2) 13.5, 12.2; 11.4 (γ-CH_3)	ca. 130[b]	−62.0, −77.0

[a]For comparison: ^{13}C resonances of $n-Pr_4PBr$ in D_2O (in ppm): 19.99(d), 14.87(s), 14.66(d). $\delta(^{31}P)$ of **1a-P**: 30.6 ppm, of **3a-P**: 34.2 ppm ($n-Pr_4PBr$ in D_2O: 32.29 ppm).
[b]Complex structure.
[c]Weak.
[d]Shoulder.
[e]Two overlapping lines.
[f]Probably of the $(CH_2)_3$ tether.
[g]$|J^{119}Sn,^{13}C|$ values between 530 and 554 Hz (for co-precipitated **1a**, **1a**, **3a**, **3a-P**, and **3b**).

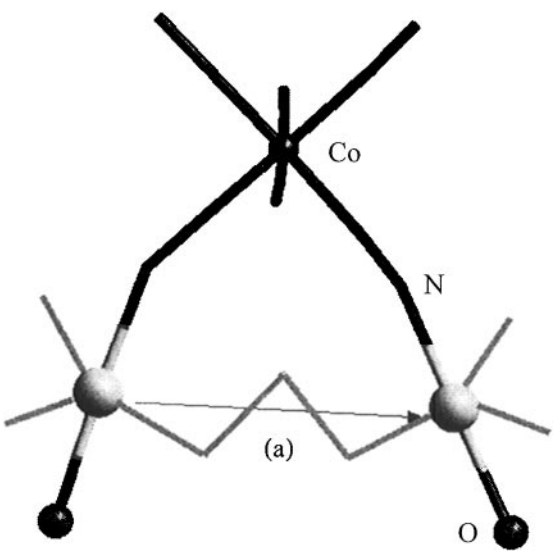

FIG. 9. Depiction of the most reasonable location of the trimethylene tether in compound **4a**.

The formation of precipitates consisting exclusively of one discrete species, and never of any mixture of different assemblies, in all cases so far studied deserves particular attention. According to all present experience, a $\{M\text{–}CN \rightarrow SnMe_3\}$ fragment may add almost equally well another cyanide ion or a water molecule. Some significant tuning of this "ambivalency" seems to be initiated in the presence of R_4E^+ ions. Mainly, but probably not exclusively, for steric reasons, the supramolecular architecture of the R_4E^+-containing assembly varies significantly with the length of the alkyl group R (8). Although R_4E^+ ions seem to promote $M\text{–}CN\text{–}SnMe_3 \leftarrow OH_2 \cdots CN\text{–}M$ bridging in favor of $M\text{–}CN\text{–}Sn(Me_3)\text{–}NC\text{–}M$ linkages, some examples of R_4E^+-free coordination polymers involving the former bonding mode are also known (24). Moreover, the extremely H_2O-rich coordination polymer $[(Et_3Sn)_3Fe(CN)_6 \cdot 20H_2O]$ prepared in our laboratory (25) is likely to contain exclusively $Fe\text{–}CN\text{–}SnMe_3\text{–}OH_2 \cdots NC\text{–}Fe$ bridges and $(H_2O)_{17}$ clusters within the large voids of its 3-D

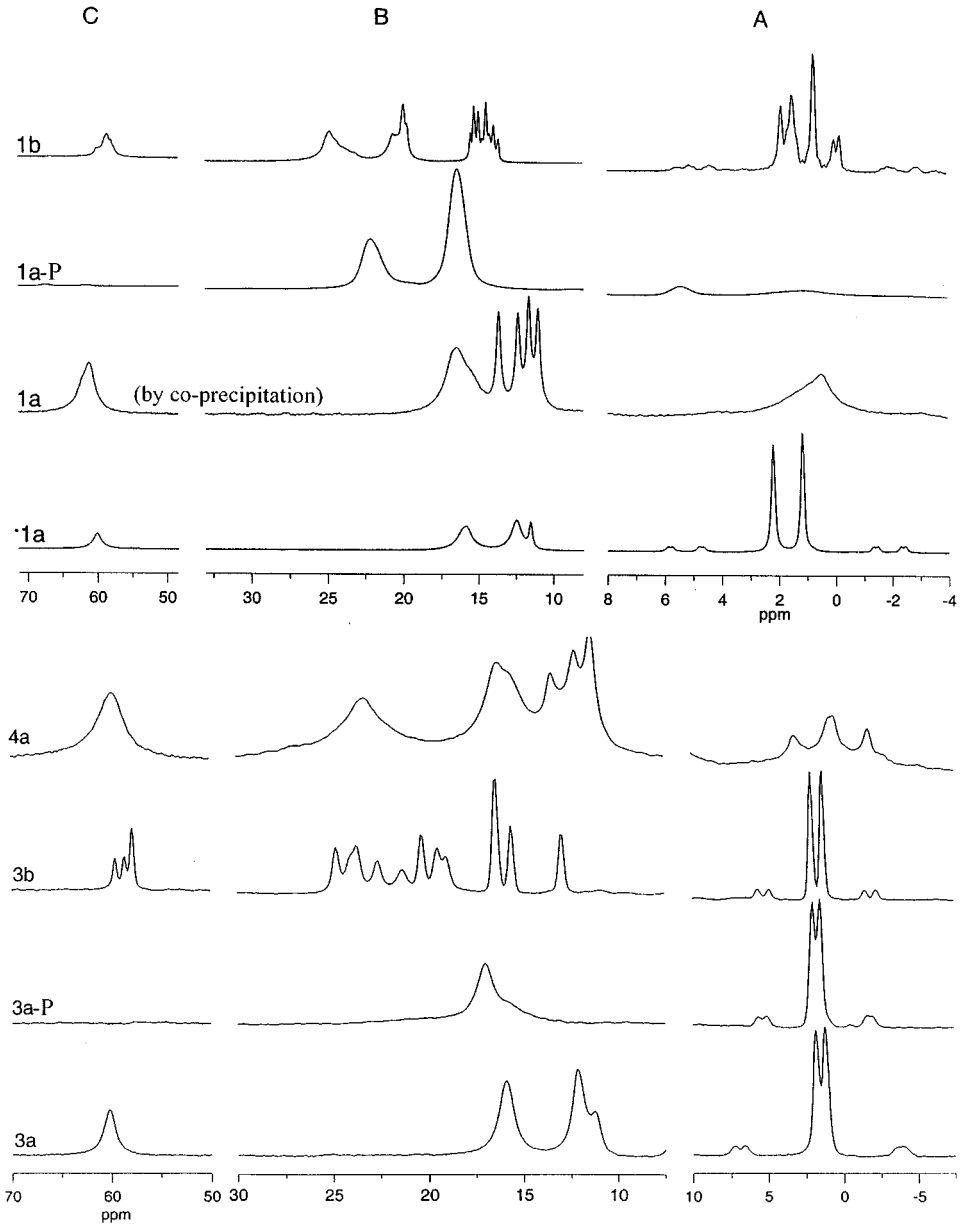

FIG. 10. ^{13}C CPMAS spectra, recorded at 75.4 MHz (except for compound **3a**, for which 50.3 MHz was used) and ambient probe temperature, for the same collection of samples as that considered in Fig. 8. Flipback of the proton magnetization was employed following signal acquisition. The spectral ranges *A*, *B*, and *C* are those for tin-coordinated alkyl groups, the alkyl carbons of the R_4E^+ ion (except the carbons in region C), and for the α-CH_2 of the R_4N^+ group, respectively. Conditions: (**1a**) Contact time, 3.00 ms; acquisition time, 89.6 ms; recycle delay, 2.0 s; spin rate, 4800 Hz; number of transients, 332. (**1a**) (co-precipitated)) Contact time, 1.00 ms; acquisition time, 60.2 ms; recycle delay, 5.0 s; spin rate, 4000 Hz; number of transients, 11,376. (**1a-P**) Contact time, 1.0 ms; acquisition time, 80.0 ms; recycle delay, 3.0 s; spin rate, 3460 Hz; number of transients, 17,064. (**1b**) Contact time, 9.0 ms; acquisition time, 80.0 ms; recycle delay, 1.0 s; spin rate, 4720 Hz; number of transients, 55,000. (**3a**) Contact time, 8.0 ms; acquisition time, 102.4 ms; recycle delay, 2.0 s; spin rate, 4000 Hz; number of transients, 40,000. (**3a-P**) Contact time, 5.0 ms; acquisition time, 100.0 ms; recycle delay, 2.0 s; spin rate, 4300 Hz; number of transients, 5682. (**3b**) Contact time, 3.0 ms; acquisition time, 100.0 ms; recycle delay, 1.5 s; spin rate, 4300 Hz; number of transients, 2444. (**4a**) Contact time, 5.5 ms; acquisition time, 50.0 ms; recycle delay, 2.0 s; spin rate, 8950 Hz; number of transients, 8810. Note that the frequency scales of the parts of this figure vary.

framework. It should, finally, be recalled that the appreciable water content of "real" Prussian blue is also due to the formation of Fe^{III}–$OH_2 \cdots$ NC–Fe^{II} interactions (the N atom being here, moreover, coordinated to another Fe(III) center) (26).

ACKNOWLEDGMENTS

This work was supported by the Deutsche Forschungsgemeinschaft (DFG), Bonn, within the Joint Project: *Nanoporous Crystals*. The CPMAS NMR spectra were obtained through the EPSRC National Solid-State NMR Service based at Durham (U.K.).

REFERENCES

1. See: (a) J. M. Lehn, "Supramolecular Chemistry—Concepts and Perspectives." VCH, Weinheim (Germany), 1995. (b) "*Comprehensive Supramolecular Chemistry*, Vol. 1" (J. L. Atwood, J. E. D. Davies, D. D. MacNicol, F. Vögtle, and J.-M. Lehn, Eds.). Pergamon, Oxford, 1996.
2. (a) R. Méric, J.-P. Vigneron, and J.-M. Lehn, *J. Chem. Soc. Chem. Commun.* 129 (1993). (b) P. C. Kearney, L. S. Mizoue, R. A. Kumpf, J. E. Forman, A. McCurdy, and D. A. Dougherty, *J. Am. Chem. Soc.* **115,** 9907 (1993), and references cited therein. (c) J. M. Harrowfield, M. I. Ogden, W. R. Richmond, B. W. Skelton, and A. H. White, *J. Chem. Soc. Perkin Trans.* **2,** 2183 (1993). (d) P. S. Bates, R. Kataky, and D. Parker, *Analyst* **119,** 181 (1994).
3. See: (a) B. M. Lok, T. R. Cannan, and C. A. Messina, *Zeolites* **3,** 282 (1993). (b) "Introduction to zeolite science and practice" (H. Van Bekkum, E. M. Flanigen, and J. C. Jansen, Eds.). Elsevier, Amsterdam, 1991. (c) "Molecular Sieves—Science and Technology" (H. G. Karge and J. Weitkamp, Eds.), Vol. 1–2. Springer, Berlin, 1999.
4. See: H. van Koningsveld and J. M. Bennett, *in* "Molecular Sieves-Science and Technology" (H. G. Karge and J. Weitkamp, Eds.), Vol. 1, p. 1. Springer, Berlin, 1999.
5. G. Thiele, J. Großmann, and A. W. Pürzer, *Z. Naturforsch.* **41b,** 1346 (1986). See also: X. Bu, T. E. Gier, and G. D. Stucky, *Acta Crystallogr. C* **52,** 14 (1996).
6. (a) U. Behrens, A. K. Brimah, T. M. Soliman, R. D. Fischer, D. C. Apperley, N. A. Davies, and R. K. Harris, *Organometallics* **11,** 1718 (1992). (b) K. Yünlü, N. Höck, and R. D. Fischer, *Angew. Chem.* **97,** 863 (1985); *Angew. Chem. Int. Ed. Engl.* **24,** 879 (1985).
7. P. Schwarz, E. Siebel, R. D. Fischer, N. A. Davies, D. C. Apperley, and R. K. Harris, *Chem. Eur. J.* **4,** 919 (1998).
8. E.-M. Poll, S. Samba, R. D. Fischer, F. Olbrich, N. A. Davies, P. Avalle, D. A. Apperley, and R. K. Harris, *J. Solid State Chem.* **152,** 286 (2000).
9. J.-U. Schütze, R. Eckhardt, R. D. Fischer, D. C. Apperley, N. A. Davies, and R. K. Harris, *J. Organomet. Chem.* **534,** 187 (1997).
10. G. W. Watt, E. P. Helvenston, and L. E. Sharif, *J. Inorg. Nucl. Chem.* **24,** 1067 (1962).
11. "Organikum," Deutscher Verlag d. Wissenschaften, Berlin, p. 203 (1988).
12. E. Siebel, (a) Diploma thesis, Univ. Hamburg, Germany, 1992; (b) Doctoral Dissertation, p. 13. Univ. Hamburg, 1998. (c) E. Siebel and R. D. Fischer, *Chem. Eur. J.* **3,** 1987 (1997).
13. J. Ascenso, H. Bai, R. K. Harris, L. H. Merwin, and J. C. Cherryman, sideband fitting program, University of Durham (1985, 1987, 1991, 1998).
14. J.-U. Schütze, Doctoral dissertation, p. 55. Univ. Hamburg, Germany, 1996.
15. E.-M. Poll, Doctoral dissertation, p. 114. Univ. Hamburg, Germany, 2000.
16. (a) M. T. Reetz, S. Hütte, and R. Goddard, *J. Am. Chem. Soc.* **155,** 9339 (1993). (b) M. T. Reetz, S. Hütte, R. Goddard, and C. Robyr, *Chem. Eur. J.* **2,** 382 (1996).
17. (a) M. Muthuraman, Y. Le Fur, M. Bagieu-Beucher, R. Masse, J.-F. Nicoud, S. George, A. Nangia, and G. R. Desiraju, *J. Solid State Chem.* **152,** 221 (2000), and references therein. (b) G. R. Desiraju and T. Steiner, "The Weak Hydrogen Bond," Oxford Univ. Press, Oxford, U.K., 1999.
18. R. Vargas, J. Garza, D. A. Dixon, and B. P. Hay, *J. Am. Chem. Soc.* **122,** 4750 (2000).
19. D. Daternieks, K. Jurkschat, D. Schollmeyer, and H. Wu, *Organometallics* **13,** 4121 (1994). M. Mehring, K. Jurkschat, M. Schürmann, H. Reuter, and D. Dakternieks, *Angew. Chem.* **109,** 1150 (1997); *Angew. Chem. Int. Ed. Engl.* **36,** 1112 (1997). M. Mehring, K. Jurkschat, M. Schürmann, I. Paulus, D. Horn, A. Orita, J. Otera, D. Dakternieks, and A. Duthie, *J. Organomet. Chem.* **574,** 176 (1999).
20. J. B. Nagy, Z. Gabelica, and E. G. Derouane, *Zeolites* **3,** 43 (1983).
21. N. Dumont, Z. Gabelica, E. G. Derouane, and L. B. McCusker, *Microporous. Mater.* **1,** 149 (1993).
22. E.-M. Poll, S. Samba, and R. D. Fischer, unpublished results.
23. Corresponding equilibria involving inter alia hydrated $\{Me_3Sn\}^+$ ions should, consequently, be responsible for exchange reactions of **1**, **2**, and **3** according to Eq. [1].
24. (a) J. Liu, W. T. A. Harrison, and A. J. Jacobson, *Inorg. Chem.* **35,** 4271 (1996). (b) E. Siebel, R. D. Fischer, N. A. Davies, D. C. Apperley, and R. K. Harris, *J. Organomet. Chem.* **604,** 34 (2000).
25. R. Tarhouni, Doctoral dissertation, p. 90. Univ. Hamburg, Germany, 1996.
26. See: (a) K. K. Dunbar and R. A. Heintz, *Prog. Inorg. Chem.* **45,** 283 (1997). (b) U. Behrens, A. K. Brimah, and R. D. Fischer, *J. Organomet. Chem.* **411,** 325 (1991).